ARKIV FÖR FYSIK Band 17 nr 7

Communicated 13 January 1960 by E. Rudberg and K. Siegbahn

Precision measurements of gamma energies and intensities by crystal diffraction

By Pär Bergvall

With 12 figures in the text

ABSTRACT

Precision measurements of gamma energies from 100 to 600 keV in the decays of ThB, Au^{198}, Sm^{153}, and Ir^{192} are reported with the following results for three strong standard reference lines:

Th B	Au^{198}	Sm^{153}
238.599 ± 0.022 keV	411.770 ± 0.033 keV	103.175 ± 0.004 keV

An efficiency calibration of the curved crystal (quartz (310), 1.5 mm thick, 2 m radius), is found to give the following energy dependence of the reflection coefficient:

$$\Gamma \sim E^{-1.99 \pm 0.10}.$$

The spectrometer efficiency is further discussed and relative intensities of some strong lines in Ir^{192} are given.

1. Short review of crystal diffraction spectrometers for gamma rays

The methods of crystal diffraction for precise energy and intensity measurements of electromagnetic radiation have for several decades been extremely successful in the field of X-rays. For measurements on gamma rays, however, the lack of sufficiently strong sources has prevented a successful application of the diffraction techniques, which are of a rather low efficiency. The development of thermal reactors with neutron fluxes above 10^{14} neutrons/sec., cm^2 has essentially removed this difficulty, and the clean and direct methods of crystal diffraction can be regarded as a valuable complement to the magnetic analysis of external and internal conversion-as well as Compton scattered electrons. In particular for the study of (n,γ) reactions, the crystal spectrometer has proved a valuable tool, competing with other types of instruments [46].

The conventional curved crystal mounting for hard X-rays, developed by Y. Cauchois, can be directly applicable to gamma rays, Fig. 1. The extended source is placed on the convex side of the crystal and gives a focussed spectrum along the Rowland circle. This arrangement is particularly suitable for photographic detec-

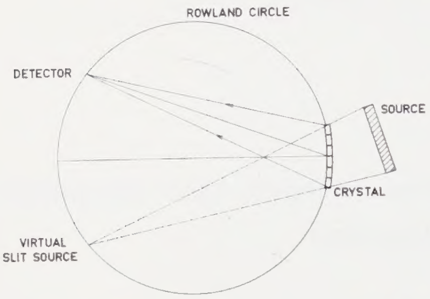

Fig. 1.

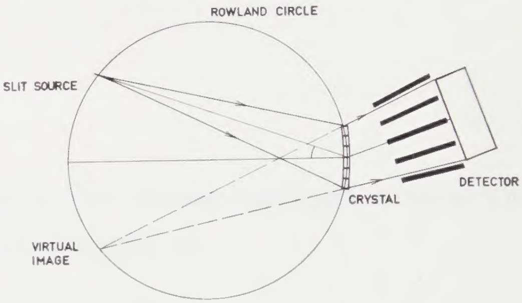

Fig. 2.

Fig. 1. The Cauchois arrangement of a curved crystal spectrometer. Photographic detection is usually employed.

Fig. 2. The Du Mond arrangement of a curved crystal spectrometer. The device is essentially a monochromator.

tion. J. W. M. Du Mond introduced a new mounting in his wellknown spectrometer by reversing the positions of the source and the detector, making use of an "inverted beam direction", Fig. 2. The instrument becomes essentially a monochromator, with comparatively high efficiency for small sources. As the spectral lines are virtual, electronic registration "point by point" is necessary. Several mechanical arrangements are possible, depending on whether the source, crystal, or detector is kept stationary while a spectrum is explored. In both the Cauchois and Du Mond arrangements it becomes necessary to use a Sollar slit, or collimator, in order to shield the detector from the direct beam at high energies. In this way, Chupp *et al.* [1] have been able to record lines of energies up to 2.2 MeV (from the $p(n,\gamma)d$ reaction) with a photographic Cauchois arrangement. The highest energy measured with Du Mond's instument so far, is 1.6 MeV [2].

Table 1. Crystal diffraction spectrometers for gamma rays.

1. Photographic Cauchois mounting.
    a. Cal. Tech., Pasadena, 2 m, quartz (310) 2 mm, Du Mond [5, 6]
    b. Univ. Cal., Livermore, same as a. Coulomb excitation work: Chupp *et al.* [6–8]
    c. Uppsala, 2 m, quartz (310) 1.5 mm, Beckman [9]
2. Du Mond mounting, fixed detector.
    a. Cal. Tech., Pasadena, 2 m, quartz (310) 2 mm, Du Mond [10]
    b. Stockholm, 1 m, quartz (310) 1 mm, Ryde and Andersson [11]
    c. Leningrad, 2 m, quartz (310) 1.6 mm, Lukirskii and Sumbaev [12]
    d. Chalk River, 2 m, quartz (310) 1 mm, gold single crystals 1 mm, Knowles [3]
3. Du Mond mounting, fixed source.
    a. Argonne N.L., 7.7 m, quartz (310) 4 mm, Hamermesh *et al.* [13]
    b. Uppsala, 2 m, quartz (310) 1.5 mm, Beckman and Bergvall [14], *this report*
    c. Techn. Hochs. München, 4.6 m, quartz (100) 3 mm, Schult [15]
4. Du Mond mounting, fixed crystal.
    a. Univ. Cal. Berkeley, 0.125 m, quartz (310) 0.2 mm, Barton *et al.* [16]
    b. Argonne N.L., 0.25 m, topaz (303) 0.2 mm, Day [17]
5. Double flat crystal spectrometer.
    a. Chalk River, calcite (211) 23 or 62 mm, Knowles [3]

For energies above 1.5 MeV, curved crystal instruments yield a rather poor resolution, > 2 %, and the efficiency is very low. The development of the double flat crystal spectrometer for nuclear spectroscopy by Knowles *et al.* [3] at Chalk River, Canada, has shown the possibilities of using crystal diffraction techniques also for MeV energies. The authors report [4] thermal neutron capture gamma rays measured in the energy region of 0.34 to 5 MeV with a nearly constant resolution of 0.5 %. By using crystals of different thicknesses in different energy regions, the efficiencies can be kept comparatively high.

In Table 1 a list of the gamma ray diffraction spectrometers in operation is given. It has been chosen to quote the radius of curvature, the crystal plane and thickness for each instrument. For further information the reader should consult the references.

2. Description of the present spectrometer construction

The principles of the present spectrometer construction have been elaborated in a previous report [14]. A detailed description of the component parts of the instrument, the adjustment and calibration procedures, and an extensive discussion of systematic errors can also be found in that report. The changes made in the construction before the present investigation are: substitution of the source slit for a source holder, removal of the monitor, and addition of a new collimator. A few important considerations will, however, be reviewed here, together with a brief general description of the instrument.

2.1. *General considerations*

In order to utilize the high resolving power afforded by the curved crystal spectrometer in the keV energy region, it is essential that the mechanical construction be of high quality. To illustrate the requirements we can cite the fact that 5 % of the half-width of a spectral line is found to correspond to only 0.005 mm on a Rowland circle of 2 m diameter. In fact, three of the spectrometers in Table 1 (2*a* and *b*, 3*a*) were at first found to possess unforeseen mechanical weaknesses, and for two of the instruments (2*c* and *d*) no precision energy measurements have yet been reported.

The object of the mechanical system is to enable a change of the Bragg angle setting while at the same time the focussing conditions are maintained. Considering the three components—source, crystal, and detector—in the Du Mond mounting, it should be realized that it is the position of the source relative to the crystal which is the most critical, as the direction of the radiation incident on the crystal surface and the crystal normal define the Bragg angle. The detector position, on the other hand, need be maintained only within the limits determined by the requirement that all of the diffracted radiation be detected. It stands to reason that a change in Bragg angle is preferably brought about by moving *only one* of the critical items (source or crystal) and the detector. Moving source and detector has been practised in the instruments 4*a* and *b* Table 1. Moving the crystal and detector has several advantages and this principle was therefore chosen for the present spectrometer construction. One advantage is that heavy shielding can be concentrated around the source, the logical place for shielding. A second advantage is the fact that the Bragg angle is given simply by half the angle of rotation of the curved crystal between the two mirror-symmetric positions of the spectrometer where Bragg reflection occurs. This angle is read off a precision circular scale with high accuracy.

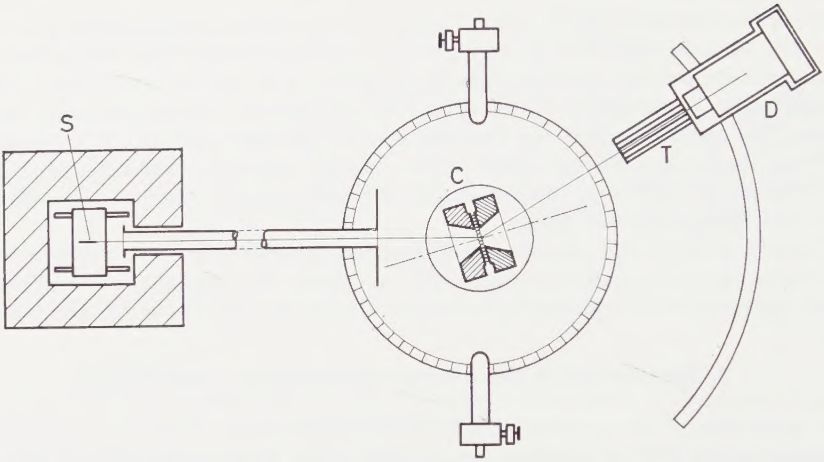

Fig. 3. Schematic drawing of the spectrometer construction. For explanation see the text.

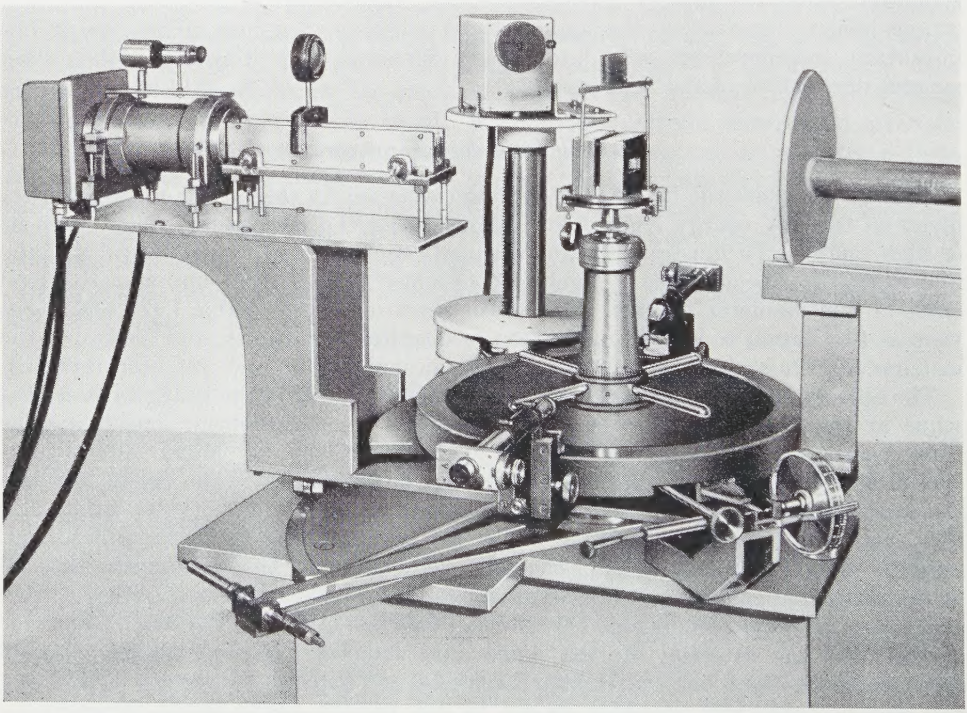

Fig. 4. Total view of the spectrometer, except for the source arrangement, which is situated to the right of the picture. The screws for the precision motion of the detector and the crystal and circular scale are visible in the lower foreground. The optical system is seen at the top of the picture, a lamp, slit and lens mounted on the detector, a mirror supported on the crystal table, and a box, seen in the background in the uppermost part of the picture, provided with a slit and housing a phototube and amplifier.

2.2. *Description of the spectrometer*

The general arrangement is drawn schematically in Fig. 3, and a photograph of the main parts, with the exception of the source holder, is found in Fig. 4. The beam travels from the source *S* in Fig. 3 to the right through a shielding lead tube, hits the curved crystal *C*, and is diffracted through the collimator *T* into the detector *D*. The source, which is self-defining, can be moved along the beam direction, which is necessary to ensure focussing for measurements below 200 keV, cf. sec. 3.1. During the actual measurements, the source is of course kept fixed. The curved crystal is made of quartz (310) with a thickness of 1.5 mm, bent to a radius of 2 m between cylindrical steel clamping blocks. The free aperture is $15 \cdot 20$ mm^2.

The collimator consists of 13 sheets of tungsten metal of dimensions $250 \cdot 20 \cdot 0.5$ mm^3, held apart by tapered brass strips along the 250 mm edges and clamped between aluminium plates. A close up view can be seen in Fig. 5. Unnecessary lead and steel shielding will only scatter and has been avoided around the collimator. The collimator transmission curve was recorded in the direct beam using Co^{60} radiation, which consists of 1.1 and 1.3 MeV gammas. As can be seen in the diagram, Fig. 6, measurements with the spectrometer should be possible up to at least 1.2 MeV without serious interference of the direct beam. The main limitation below this

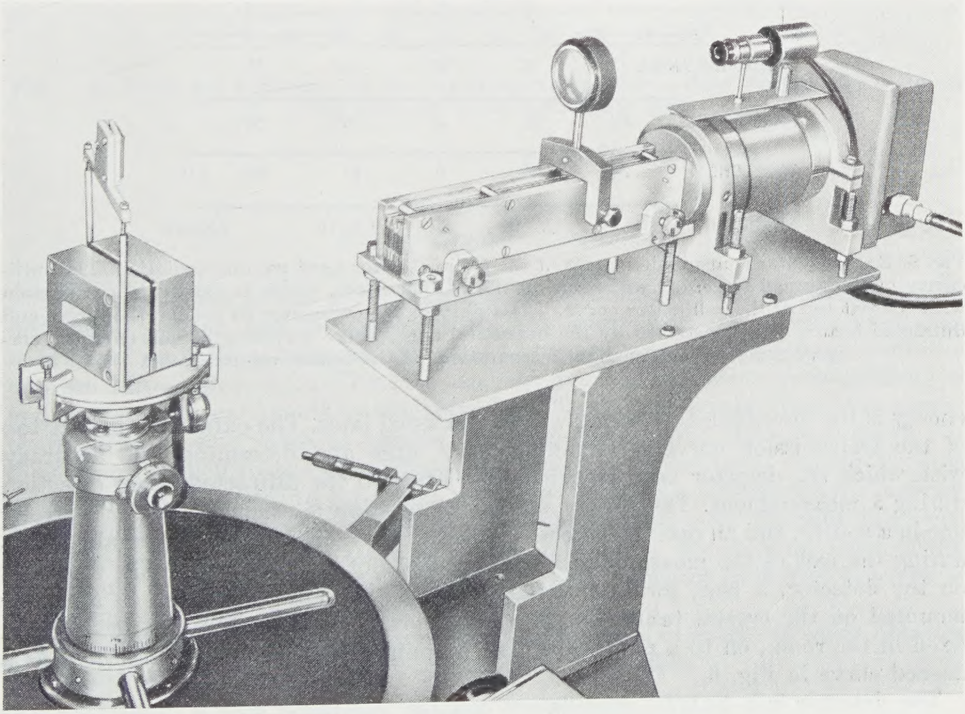

Fig. 5. Close up view of the crystal table and detector arrangement. The beam travels from the left to the right in this picture.

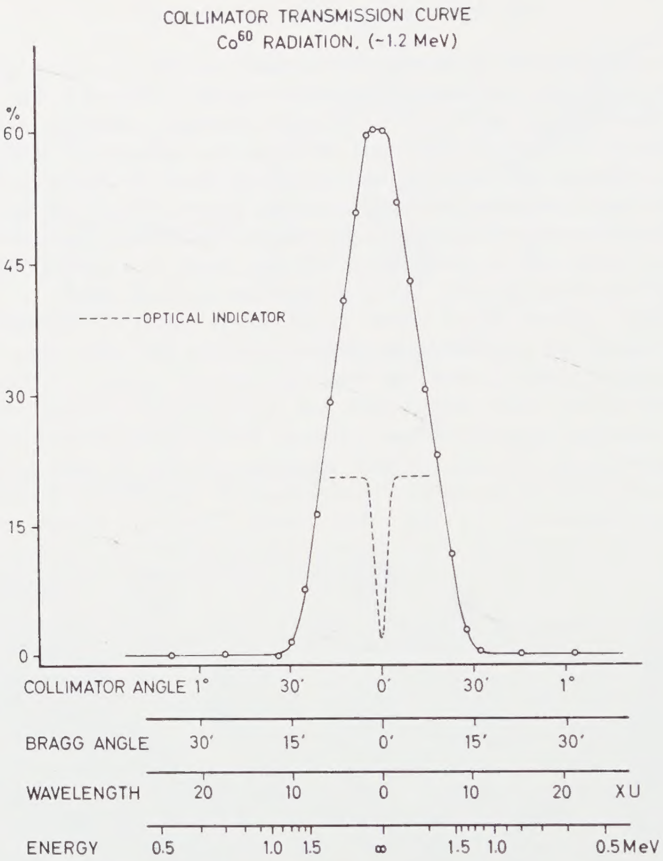

Fig. 6. Experimental transmission curve of the collimator for hard gamma radiation. The sufficiency of the optical system is witnessed by the dashed curve, which is narrow in comparison with the flat top of the collimator curve. The ability of the collimator to resolve the direct and diffracted beams is demonstrated by the horizontal axes, where wavelengths and energies, corresponding to various angular separations of the beams, are indicated.

energy is the low efficiency, which will be discussed later. The extent of the flat top of the transmission curve is advantageously large and determines the accuracy with which the detector need be oriented relative to the diffracted beam direction during a measurement. The correct collimator position is easily found for a strong line in a source, and an optical system, visible in Fig. 4, ensures the proper alignment during the rest of the measurements. This consists of an illuminated slit, mounted on the detector, a lens, forming an image of the slit after reflection in a mirror mounted on the crystal table. The image is allowed to fall through a second slit, fixed in the room, on to a phototube. The amplified photocurrent is indicated as a dashed curve in Fig. 6.

The detector is a NaI(Tl) scintillation counter, combined with a linear amplifier and differential discriminator. The electronics were built by Dr Åström at the Nobel Institute in Stockholm.

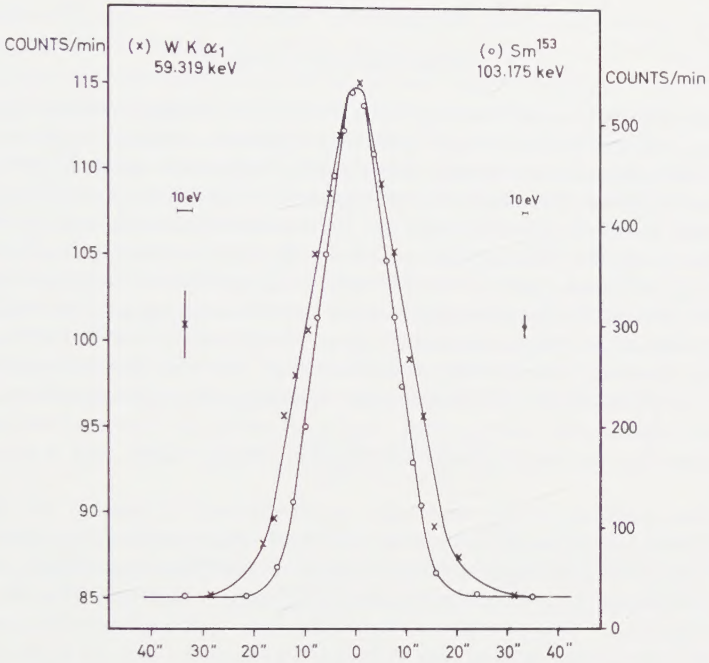

Fig. 7. An X-ray and a gamma- ray line superimposed in order to show the influence of natural line width on the spectral line shape.

2.3. *Spectrometer resolution*

The spectral line widths are determined by focal aberration, the intrinsic crystal diffraction pattern, and the source width. The source width is always chosen close to 0.1 mm, an optimal value as it is equal to the combined width of focal aberration and the diffraction pattern. This fact has been found in a previous investigation [18] and agrees with predictions by Sumbaev [19]. The source height gives only a small contribution to line width as vertical divergence effect, and the source depth (the dimension parallell to the beam direction) gives an equally small contribution due to defocussing. In order to get a high counting rate with a limited specific activity, a strip source of dimensions $15 \cdot 4 \cdot 0.1$ mm^3 is conveniently used. The total line width for a gamma ray from such a source is 16″ (seconds of arc). For an X-ray line a further broadening is caused by natural line width. This is apparent from Fig. 7, where an X-ray and a gamma line are superimposed.

The variation of the spectrometer resolution in terms of energy is easily obtained by differentiation of eq. (2), and is given by the expression:

$$\frac{\Delta E}{E}\,(\%) = 1.4 \cdot 10^{-3} E\,(\text{keV}). \qquad (1)$$

3. Energy measurements

3.1. *Experimental procedure*

The source is usually a self-limiting strip of material, which is sandwiched between machined aluminium plates before activation. Such a capsule, once activated, is placed in a slot in the source holder, where tightening screws serve to give the source a well-defined position and alignment. The source holder is then slid into the proper position for the source to coincide with the Rowland circle for the energy region to be explored. The method of finding this position ("Hartmann tests") has been described previously [14]. For energies above 200 keV, this position is one and the same. A pulse height spectrum is then recorded in the direct beam, giving information on the optimal adjustment for the discriminator channel of the detector. With the collimator in the correct bearing, the curved crystal is swept over the interesting angle region in steps of 2 to 3 seconds of arc, the angular positions are read and counts are taken. A line profile delineated, the crystal (and collimator) is swung to the mirror-symmetric position by turning through the double Bragg angle, and a second profile is recorded.

The angular positions of the lines can be established by taking the diameter of horizontal chords. An alternative method is that of superposition of profiles, discussed by Muller *et al.* [20]. The angular displacement of the lines required to bring about the closest overlapping, is then determined, judging by the eye. The advantage, in point of principle, of this procedure lies in the fact that asymmetries in line shape caused by the source and crystal, are reflected in the same way in both profiles, and do not influence the angle measurement. Both the above methods have been found to yield the same results for lines recorded with the present spectrometer. It is namely of no consequence if the superposition is carried out literally, or just by establishing the line positions in the same way for both profiles, the existing asymmetries reduce in importance by the mere fact that two identical profiles are employed.

Bragg's law will now give the wavelength λ from knowledge of the diffraction angle θ. It is, however, necessary to carry out a calibration, determining the atomic spacing d of the crystal plane employed:

$$\lambda = 2d \sin\theta. \tag{2}$$

For the calibration a standard X-ray line, preferably of low energy to permit a high relative accuracy, is used. As has been discussed at length previously [14], the value of d thus obtained includes allowance for several systematic errors with a *linear* wavelength dependence. The calibration constant is to a slight extent dependent on the exact geometrical alignment of the crystal, and the calibration should be repeated after a readjustment of the spectrometer. The gamma-ray wavelengths will be obtained in X-units. The conversion constant to keV is given by Cohen and Du Mond [47]:

$$12372.44 \text{ keV}\cdot\text{XU}.$$

3.2. *Error estimate*

The limits of accuracy of measurements with the present instrument are primarily determined by the quality of the circular scale. From previous X-ray measurements, using different parts of the scale and comparing with the results from other laboratories and data obtained with different methods [14, 18, 21–23], it can be concluded that the systematic errors in one angle reading is less than 0.2″. This means for an angle measurement (the difference between two angle readings), $0.2\sqrt{2}''$, and for a Bragg angle, which is half the measured angle, about 0.15″. It should be noted that a reading always involves a check on five consecutive scale divisions.

The accidental errors associated with the determination of a line position are connected with the reproducibility in the angle readings and count statistics. Experience from previous X-ray measurements with very good count statistics has shown [21] that the standard deviation in line position amounts to 1/80 of the line width at half maximum intensity. This still applies to strong gamma rays. An estimate of the standard deviation in line position, caused by statistical fluctuations, has been given by Muller *et al.* [20]. Muller's formula has been derived to apply to the method of profile superposition, but can be used with sufficient approximation in the present case. The standard deviation in Bragg angle, $\pm\sigma$, is given by the formula:

$$\sigma^{-2}=\frac{4HT}{W^2}\ln\left(\frac{H+B}{B}\right) \tag{3}$$

W is the base width of the line (assumed triangular) in angular measure, H and B are its peak height and background height (in counts per unit time) and T is the total aggregate of counting time expended in determining the points on the profiles. As

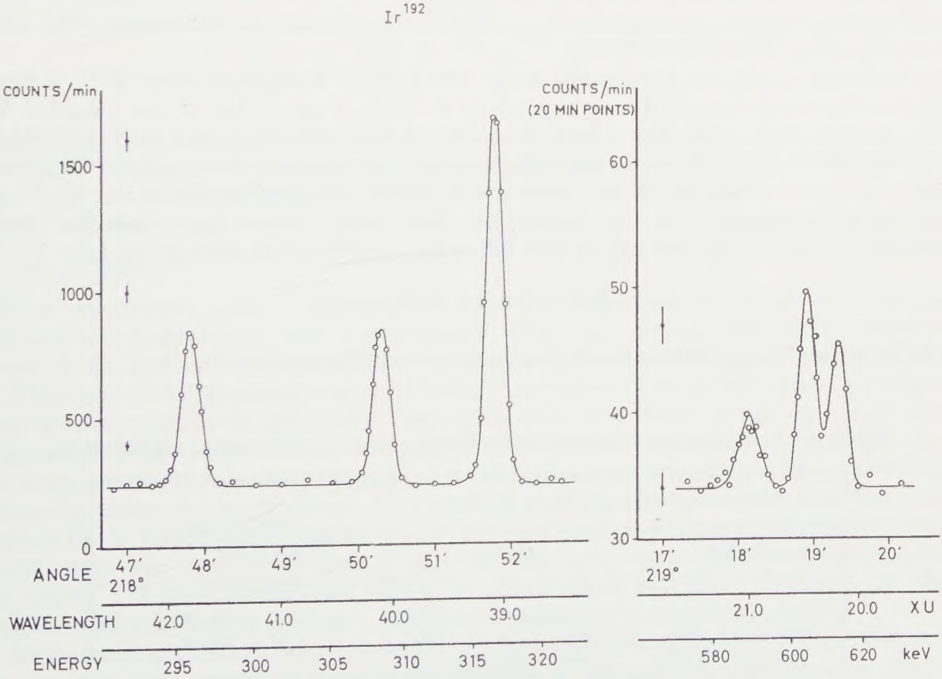

Fig. 8. Two regions in the spectrum of Ir^{192} around 300 and 600 keV. The 613 keV line represents the highest energy recorded so far with the instrument. Count statistics are indicated. The total source strength is about 340 mC.

expected, σ becomes negligible for the strong lines, such as the 300 keV group in Fig. 8, but for weak lines good agreement has been found with the observed reproducibility. If n measurements are made, the standard deviation for the mean is found by division of σ by $\sqrt{n}$. The errors assigned in Bragg angle are double standard deviations, quadratically added to the systematic error allowance. A calibration error of 27 ppm is finally included in the wavelength and energy errors given.

It should be pointed out that the procedure of fitting a curve to a number of points with poor statistics, such as those in Fig. 9, is simplified by the fact that line shape and width are the same in the two spectrometer positions, and the same for weak and strong lines from the same source. The profiles are always symmetrical, providing, of course, that they contain only one gamma energy.

3.3. *Experimental results*

a. *Calibration, W* $K\alpha_1$

Before the present investigation took place, the conical shaft of the precision circle was re-oiled. A subsequent readjustment of the spectrometer was made, and a recalibration was therefore required.

W $K\alpha_1$ can be regarded as one of the best established X-ray lines. It has been measured by three authors, relative to Mo $K\alpha_1$, a line which is closely connected to the definition of the X unit by several high precision determinations in different laboratories. The W $K\alpha_1$ wavelength measurements are reviewed in Table 2. The unweighted mean is the same value as that recommended by Sandström [26], and has been used in this calibration.

The source used was a tungsten strip, which upon activation gives W^{187}, a beta emitter which produces a fairly high yield of W K X-rays. One of the recorded W $K\alpha_1$ profiles is shown in Fig. 7, and the results of the calibration are found in Table 2.

It should be noted that thermal expansion of the quartz crystal makes a temperature correction necessary if the subsequent energy measurements are not made at the same temperature as the calibration. The Bragg angles have therefore been reduced to 18°C with the aid of the following correction in seconds of arc:

$$\Delta\theta'' = 3.0\ (t - 18.0)\ \mathrm{tg}\ \theta. \qquad (4)$$

t is the mean temperature and the correction is applied with sign.

Table 2. Previous measurements of W $K\alpha_1$ and spectrometer calibration.

Previous measurements of W $K\alpha_1$		Calibration Bragg angle, 18°C
λ, XU	Author	
208.571 ± 0.010 208.575 ± 0.008 208.572 ± 0.004	Ingelstam [24] Watson *et al.* [25] Beckman *et al.* [14]	5° 4′ 51.8″ 5° 4′ 52.0″
Mean: 208.573	cf Sandström [26]	Mean: 5° 4′ 51.9″ ± 0.5″ *d*: 1177.51 ± 0.03 XU

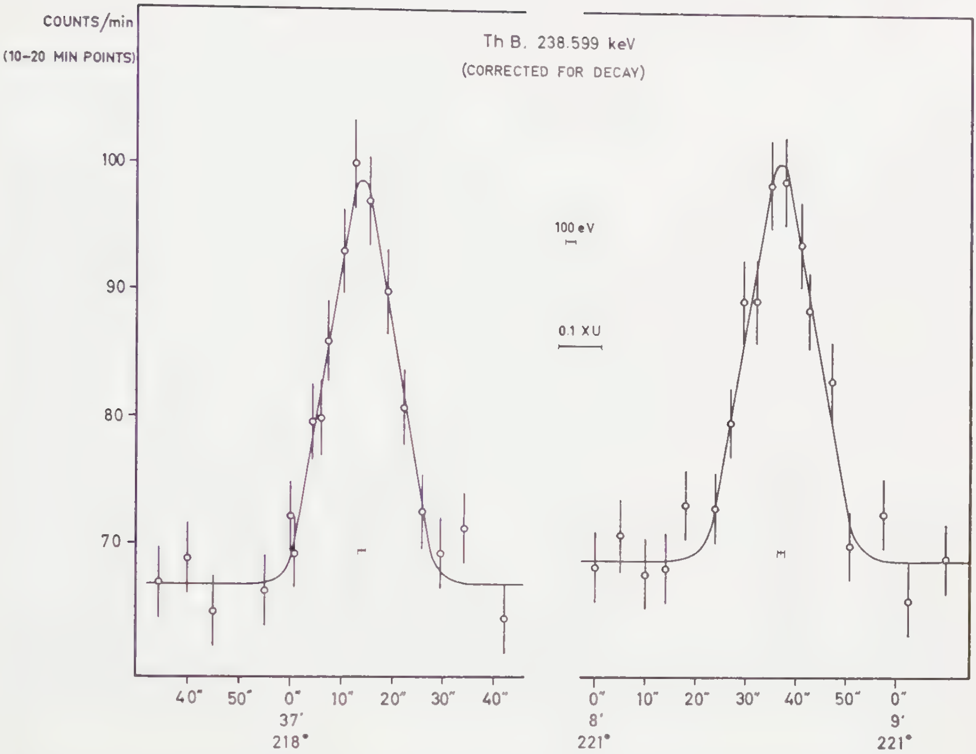

Fig. 9. The Th B line as recorded in the two positions of the spectrometer after correction for decay. The errors, double standard deviations, in profile position, caused by count statistics according to eq. (3) are indicated at the base of the lines.

b. *Th* $B(Pb^{212})$

The conversion lines following the Th $B \rightarrow C$ transition are frequently used as calibration standards in beta spectroscopy. Only one crystal diffraction measurement of the gamma lines has so far been made, by the Du Mond group in 1952 [20].

The source was prepared from a radiothorium source of 20 mC strength by collecting the active, gaseous radon as a deposit on a 0.1 mm thick monel wire, held at a high negative potential. The short half-life of the lead isotope, 10.6 hours, made corrections for decay especially important in this case, particularly in view of the long counting times; it took 10 hours to cross both profiles. The background without the source in the spectrometer (which was 85 % of the total background during the measurements), was first determined accurately and later subtracted from the number of counts obtained during the recording. Each point was then corrected for the exponential decrease in intensity, the resulting profiles being shown in Fig. 9.

Four measurements of the strongest line are reported in Table 3. The first two were made with rather poor statistics, rendering the results a low weight. For a comparison of the present result with previous beta spectrometer data, the F and I conversion line energies have been calculated by subtraction of the K and L_{I} binding

Table 3. Th B (Pb^{212}) measurements.

Bragg angle 18°C	Weight	Wavelength XU	Energy keV
1° 15′ 42.5″	1	51.859	238.578
1° 15′ 41.1″	1	51.843	238.652
1° 15′ 42.3″	4	51.857	238.589
1° 15′ 42.0″	4	51.853	238.604
Mean: 1° 15′ 42.1″ ± 0.4″		51.854 ± 0.005	238.599 ± 0.022

Table 4. Comparison between present and previous Th B data, energies given in keV.

	Present	Muller *et al.* [20]	Siegbahn *et al.* [27]	de Vries [28]
Gamma line	238.599	238.595 ± 0.032	—	—
F-line	148.066	—	148.08 ± 0.02	148.05 ± 0.03
I-line	222.204	—	222.21 ± 0.03	222.18 ± 0.05

energies of Bi according to ref. [24, 26, 29]. The agreement is seen from Table 4 to be very good, and it should be noted that the present measurements, although performed on a very weak line, are nevertheless of a higher relative accuracy than the most precise beta spectroscopic data available.

c. Au^{198}

The 412 keV line in Au^{198} is a frequently used calibration line [11]. It was measured here with the use of a gold source of about 1 *C* strength, giving a peak counting rate of 2500 counts per minute and a signal to backgound ratio of 12. Four measurements were made, reported in Table 5, together with the previous result by Muller *et al.* [20]. It should be reassuring for those who have been using the older value to note that the agreement is excellent.

d. Sm^{153}

The strong 103 keV line in Sm^{153} is suitable for the efficiency calibration of the curved crystal. As it is also used as a calibration line by beta spectroscopists at this

Table 5. Present and previous measurements on Au^{198}.

Bragg angle 18°C	Wavelength XU	Energy keV	Muller *et al.* [20] keV
43′ 51.5″	30.0442	411.808	411.770 ± 0.036
43′ 52.2″	30.0519	411.702	
43′ 51.6″	30.0452	411.794	
43′ 51.7″	30.0464	411.778	
Mean: 43′ 51.8″ ± 0.2″	30.0470 ± 0.0024	411.770 ± 0.033	

Table 6. Present and previous measurements on Sm^{153}.

Bragg angle 18°C	Wavelength XU	Energy keV	Previous keV
2° 55′ 7.7″	119.919	103.173	Beckman [9]: 103.18 ± 0.04 Andersson [30]: 103.27 + 0.02
2° 55′ 7.4″	119.916	103.177	
Mean: 2° 55′ 7.6″ ± 0.3″	119.917 ± 0.004	103.175 ± 0.004	

Table 7. Gamma ray- and conversion electron energies, and conversion electron momenta of standard lines.

Parent nucleus	Gamma energy keV	K conversion		L_I conversion	
		keV	Gauss-cm	keV	Gauss-cm
Th B	238.599 ± 0.022	148.066 ± 0.023	1388.37 ± 0.11	222.204 ± 0.023	1753.85 ± 0.09
Au^{198}	411.770 ± 0.033	328.662 ± 0.034	2222.39 ± 0.12	396.921 ± 0.034	2503.25 ± 0.11
Sm^{153}	103.175 ± 0.004	54.652 ± 0.004	809.12 ± 0.03	95.118 ± 0.004	1087.31 ± 0.02

institute, an energy determination was carried out. The two previous crystal diffraction measurements of this line are namely in strong disagreement [9, 30]. A typical profile is shown in Fig. 7, and the results are given in Table 6.

For the benefit of beta spectroscopists, a summary is given in Table 7 of the measurements on Th *B*, Au^{198} and Sm^{153}, in terms of gamma energies as well as conversion electron energies and momenta. The atomic binding energies are obtained, for Bi from photo electron data on the L_{III} level by Sokolowski [29] together with X-ray data from Sandström [26], for Hg likewise from Sokolowski [29] and Sandström [26] although the *K* level is computed from X-ray measurements by the present author [48]. In Eu, the present author has together with Hagström [22], made photo electron and X-ray measurements which give the *K* and *L* levels. The conversion from electron energy to momentum has been carried out with the aid of the tables by Gerholm [49] which enable high accuracy as they permit interpolation to second order.

e. Ir^{192}

Ir^{192} is a source with a long half-life and which can be obtained in high strength. It contains several lines of different energies and is ideal for testing and adjusting the spectrometer. The energies and intensities of the emitted gammas have been measured previously by several authors. The source used in this investigation, a 120 mg strip, was activated to a strength of 340 mC. Part of the spectrum is shown in Fig. 8. The energy measurements, together with previous data, are reported in

Table 8. Present and previous measurements on Ir^{192}.

Daughter nucleus [32]	Bragg angle 18°C	Mean values of Bragg angle Wavelength, XU Energy, keV	Previous data, keV Ryde *et al.* [11] Muller *et al.* [20]
Pt^{192}	29′ 28.2″ 29′ 28.8″	29′ 28.5″ ±0.7″ 20.191 ±0.008 612.77 ±0.25	— 612.87 ±0.61
Pt^{192}	29′ 51.8″ 29′ 53.3″	29′ 52.6″ ±0.7″ 20.466 ±0.008 604.54 ±0.24	— 604.53 ±0.59
Pt^{192}	30′ 39.0″ 30′ 39.7″	30′ 39.4″ ±0.7″ 21.000 ±0.008 589.16 ±0.23	— 588.40 ±0.28
Pt^{192}	38′ 35.5″ 38′ 34.8″ 38′ 34.8″	38′ 35.1″ ±0.3″ 26.432 ±0.003 468.09 ±0.05	467.95 ±0.12 467.984 ±0.061
Pt^{192}	57′ 3.6″ 57′ 3.5″ 57′ 4.6″	57′ 3.9″ ±0.3″ 39.090 ±0.003 316.512 ±0.020	316.52 ±0.04 316.462 ±0.034
Pt^{192}	58′ 33.2″ 58′ 33.6″	58′ 33.4″ ±0.3″ 40.112 ±0.003 308.447 ±0.022	308.66 ±0.06 308.454 ±0.033
Pt^{192}	1° 1′ 1.5″ 1° 1′ 1.8″	1° 1′ 1.7″ ±0.3″ 41.804 ±0.003 295.963 ±0.021	295.96 ±0.10 295.942 ±0.031
Os^{192}	1° 27′ 46.1″	1° 27′ 46.1″ ±0.5″ 60.118 ±0.006 205.803 ±0.021	— 205.736 ±0.038
Os^{192}	1° 29′ 44.1″	1° 29′ 44.1″ ±0.5″ 61.466 ±0.006 201.289 ±0.020	— 201.306 ±0.037

Table 8. A support for the present data can be found by adding up cascading gammas and comparing with the crossovers according to the decay scheme in ref. [45]. If the energy value of a weak, low energy line is taken from Muller *et al.* [20], three such relations can be found, presented in Table 9.

Table 9. Energy relations between transitions in Pt^{192}.

Sum of cascading energies, keV	Crossover energy, keV
295.963 + 308.447 = 604.41 ±0.04 136.33* + 468.09 = 604.42 ±0.05 295.963 + 316.512 = 612.48 ±0.04	604.54 ±0.24 612.77 ±0.25

* Taken from ref. [20].

4. Intensity measurements

The relative intensities of the gamma rays are obtained in the following way. The spectrometer is set at the Bragg angle corresponding to the peak of a line being studied, and the pulse height spectrum of the NaI scintillation detector is recorded. By changing the Bragg angle by the small amount required to depart from the line profile, the background, arising mainly from the influence of the direct beam, can be recorded and subtracted. The total number of counts recorded in the photopeak is then proportional to the relative intensity of the gamma line after corrections for absorption, curved crystal reflectivity and detector efficiency are applied. Because of the energy dependence of the detector resolution, the area under the photopeak rather than the maximum counting rate should be used. The mentioned corrections will now be discussed in turn.

4.1. *Absorption*

Attenuation of the radiation by absorption in the spectrometer takes place mainly in the curved crystal and is rather small, less than 3 % for energies above 100 keV. The self-absorption in the source, however, constitutes a much more serious problem. In order to make the absorption corrections small and easily calculable, the source should be in the form of a wire, or, as a powder, packed in a capillary tube. At present it is not possible to obtain the high specific activities required in such an arrangement. Instead, strips of material, $15 \cdot 4 \cdot 0.1$ mm^3 in size, were used, yielding up to 40 times the intensity obtainable from a 0.1 mm thick wire of the same specific activity.

The absorption corrections were calculated using the following formula:

$$\frac{I}{I_0} = \frac{1 - e^{-\mu d}}{\mu d}. \tag{5}$$

The source depth d equals 4 mm, and values of the linear absorption coefficient μ were computed from data given in ref. [33]. For the iridium source used, the absorption varies from 95 % at 100 keV to 37 % at 600 keV. For a rigorous application of these corrections it becomes important that the strip be accurately aligned with respect to the beam direction, which may be rather difficult to accomplish. A way to surmount these difficulties is to use sources of different depth for measurements in different energy regions.

4.2. *Reflecting properties of the curved crystal*

a. *Previous work*

The reflecting properties of an elastically bent crystal in the (Laue) transmission case have been investigated by several authors. The first extensive experimental and theoretical studies of this problem were made by the Pasadena group in the dissertation work carried out by Lind and by West, unpublished but summarized by Lind, West, and Du Mond [34] in 1949. Employing the same crystal plane as the one used in the present work, quartz (310), in a 1 mm thick lamina, curved to 2 m radius, those authors found that the integrated reflection coefficient R_θ varied inversely as the square of the energy of the reflected radiation. This behaviour was known to be characteristic of a mosaic crystal assuming low primary and secondary extinction.

The reason for this behaviour remained obscure but it was generally believed that the bent crystal consisted of a mosaic of a number of finite perfect domains. It was shown by Sumbaev [35] in 1957, however, that the complete expression for R_θ could be derived from the theory of elasticity of an anisotropic body.

The experimental evidence for an E^{-2} dependence of R_θ by Lind, West, and Du Mond covered the region of 25 keV to 1.3 MeV. In 1956, Hatch [36], using an improved technique, verified the same energy dependenc for a crystal of double the thickness. The E^{-2} power law was generally accepted by various authors, for instance Beckman [37], and Jaffe *et al.* [38], in relative intensity measurements. Day [17], however, working with the small Argonne instrument, reported the exponent to be -1.35 for topaz (303) in the energy region of 50 to 80 keV. Cochran and Ross [39] measured R_θ for a mica crystal for low energies and found an $E^{-1.9}$ dependence for energies above 25 keV. For energies decreasing below this value, the exponent was found to increase through zero to positive values below 15 keV. The authors interpret their findings as the influence of increasing secondary extinction and conclude that it will be necessary to carry out a direct calibration of a curved crystal over the actual range of energies within which intensity measurements are to be made. Sumbaev [12] reports a value for the exponent of -1.85 ± 0.04 for quartz (310) 1.6 mm thick, in the energy region of 152 keV to 1.23 MeV as a result of measurements with the Leningrad spectrometer. Schult [15], in his thesis, describing the diffraction instrument in München, presents a thorough discussion of the problem and reports experimental evidence of a E^{-2} dependence of quartz (100), 1 mm thick, for high energies and weak reflections, whereas for low energies and strong reflections, an "ideal" E^{-1} behaviour is found. Finally, Edwards in a recent, not yet published thesis work [40] on Du Mond's instrument in Pasadena, has measured the energy dependence of R_θ employing two different methods. He reports the values for the exponent:

$$-1.963 \pm 0.027 \text{ and } -1.999 \pm 0.020, \text{ mean value } -1.986 \pm 0.016.$$

In view of the close similarity between the crystal employed in the present instrument and in that of Du Mond, one should expect Edwards' results to hold in the present case too. The necessity for an independent calibration is, however, apparent.

b. *Experimental procedure*

The technique used here is the same as that employed by Lind, West, and Du Mond [34] and which is followed by all the above authors. The detector is placed in the direct beam and a pulse height spectrum is recorded. The photopeaks should be well resolved, and the intensity I_0 of a particular energy is established. The spectrometer is then set on the diffraction peak of this energy, and a second pulse height spectrum, intensity I_b, is recorded under otherwise unaltered conditions. It should first be noted that the geometry, absorption and detection conditions are identical except for the fact that we first record the direct, and then the diffracted beam. The following ratio

$$\Gamma = \frac{I_b}{I_0} \tag{6}$$

is consequently a measure of the reflection power of the crystal, usually called the reflection coefficient. It has been shown by Lind that under certain simplifying assumptions one obtains:

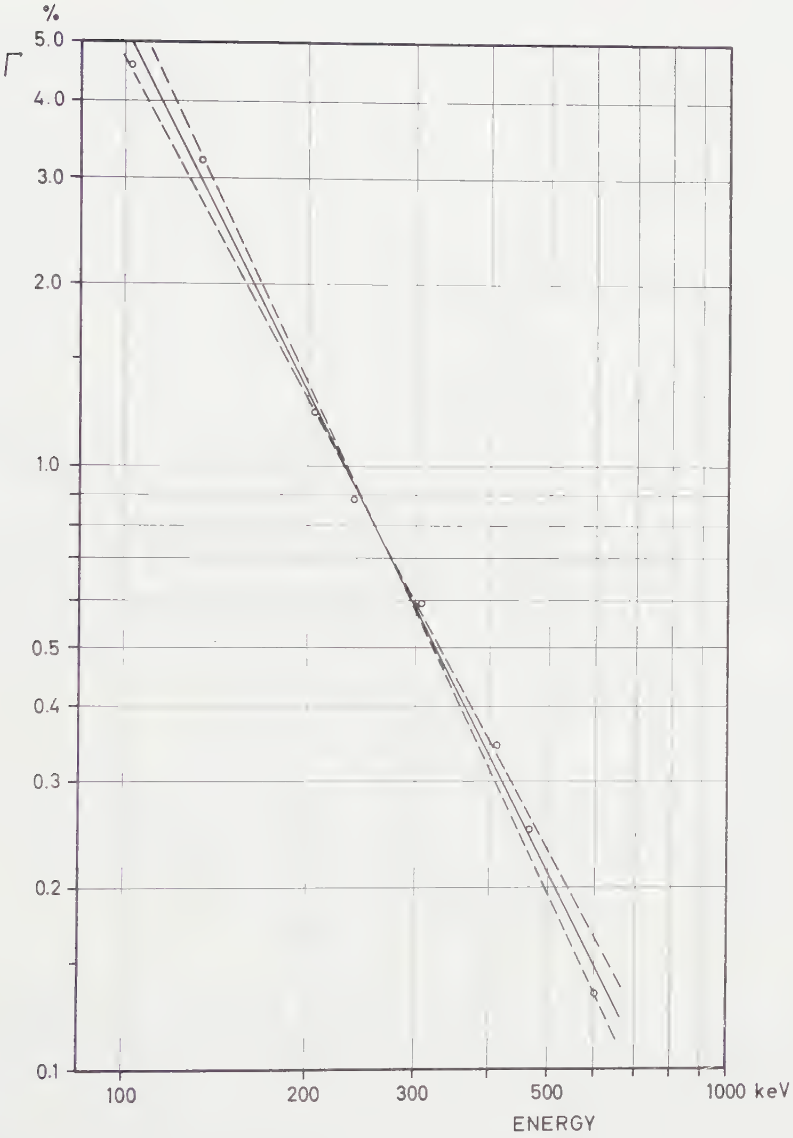

Fig. 10. The reflection coefficient, Γ in eq. (6) of the curved crystal for 0.1 mm source width.

$$R_\theta = \frac{t}{\varrho} \Gamma. \tag{7}$$

Here t is the source with and ϱ the radius of curvature of the crystal. The assumptions are the following [34]: The linear extension of the focal aberration pattern, w_1, and the width of the source, t, on the focal circle are approximately equal and are large compared with the intrinsic crystal diffraction pattern width w_2 and the width w_3

of the spectral distribution. For gamma radiation, w_3 is always negligible, and for the present instrument it is known [18] that the combined width of w_1 and w_2 is approximately equal to a width t of 0.10 mm. It has been generally assumed that for quartz (310) in the stressed state, w_2 is only a few seconds of arc and thus much smaller than w_1, which should give the main contribution to the spectrometer window besides t. This has been criticized by Sumbaev [19], claiming that w_2 is large and actually proportional to the thickness of the crystal lamina. An optimal value for w_2, equal to a source width $t = 0.1$ mm, is reached already for a crystal thickness of 1.4 mm (assuming 2 m radius). In order not to rely on eq. (7) too much, sources of as close to equal width as possible were used in the present calibration. With the aid of a microscope the source widths were determined to be 0.10 mm within 5 %. The samarium source width was determined by weighing. Eq. (7) was then used only for the slight correction of Γ to 0.10 mm source width.

For close-lying groups of lines, such as those in Fig. 8, which were not resolved in the pulse height spectra in the direct beam, the intensity I_0 was divided according to the relative intensities of the lines, and the I_b/I_0 ratio calculated for the strongest line in each group.

In the logarithmic diagram, Fig. 10, Γ is plotted as a function of energy E for eight recorded lines in Sm^{157}, W^{187}, Ir^{192}, Au^{198}, and ThB (Pb^{212}). The straight line is drawn according to a least squares fit, and the slope is found to be -1.987. The standard deviation is calculated from the displayed scatter of the experimental point and equals 0.049. As an error estimate 0.10 was chosen, corresponding to a confidence coefficient of 90 %. The asymptotes of the confidence band are drawn in the figure. The following result is obtained:

$$\Gamma = \text{const.} \cdot E^{-1.99 \pm 0.10}. \tag{8}$$

This applies only to the energy interval of 100 keV to 600 keV. As lower and higher energies are measured in the future, new points will be added to the calibration curve.

4.3. *Detector efficiency*

The efficiency calibration of a NaI scintillation detector has been exhaustively discussed by many authors (see for instance [41]), and can now be regarded as a standard procedure. Curves for the total absorption coefficient for various energies can be found in the literature [42]. Efficiencies for different source and crystal geometries are calculated and tabulated in ref. [43]. It is, however, a wellknown fact that photoelectric absorption data, taken from the literature, cannot be used to represent the area under the photopeak in a pulse-height spectrum. This is so because also the Compton scattered photons may be trapped in the crystal by secondary processes, and consequently the entire energy of the gamma quantum will be registered, viz. in the photo peak. Experimental determinations of the "peak to total ratio" are therefore required for each specific geometry. This is usually done employing essentially monochromatic gamma ray sources, see for instance ref. [44].

The calibration procedure in the present case is simplified in two respects. First, the source is so far removed from the NaI crystal (about 100 times the crystal dimensions), that the incident beam may be considered parallel. No edge effects need therefore be considered. Second, the curved crystal may serve the purpose of selecting a particular energy, even from a complex spectrum, so that strictly monochromatic pulse height spectra for the detector can be obtained for any energy which is measured.

In Fig. 11 the result of the calibration is represented. The solid line gives the total absorption according to ref. [42]. The dashed line has been obtained as the product of the total efficiency and experimentally determined peak to total ratios. Due to the lack of a sufficiently strong source in the high energy region, the 660-keV point was obtained with the aid of Cs^{137} radiation, which is essentially monochromatic, in the direct beam. The curves show that the present scintillating crystal (cylindrical shape, 1″·1″) seriously reduces the spectrometer efficiency at higher energies. Substitution of a larger crystal will easily overcome this unnecessary limitation.

4.4. *Experimental results of relative intensities*

Relative intensity measurements on Ir^{192} carried out and corrected according to the above paragraphs, are given in the first column of Table 10. In view of the large and uncertain self-absorption corrections, only lines of energies above 290 keV are reported. As a comparison are given two sets of data obtained by curved crystal instruments, according to Sumbev [12] and the Du Mond group [20]. Three sets of measurements on external conversion electron intensities by magnetic spectrometers are also included. The agreement is satisfactory (excepting ref. [20]) considering the poor statistics at the highest energies in the present work (cf. Fig. 8).

5. Total efficiency of the spectrometer

In the preceding paragraphs the energy-dependent factors determining the spectrometer efficiency were discussed. For an estimate of the total efficiency we shall consider two more factors of geometrical nature.

By the total efficiency we shall mean the ratio of two factors. The numerator is the peak counting rate of a diffraction line, obtainable using sufficient channel width to encompass the photopeak. This number is further corrected to zero self-absorption, which means that we assume a source of small depth and high specific activity. The

Table 10. Present and previous measurements of relative intensities from the decay of Ir^{192}.

Energy keV	Crystal diffraction			External conversion electrons		
	Present	Sumbaev [12]	Muller* *et al.* [20]	Baggerly *et al.* [32]	Johns, Nablo [31]	Bashilov *et al.* [50]
296	34.5	37.0	38.3	35.9	33.9	39.0
308	38.0	37.9	37.2	34.9	36.4	40.3
317	100	100	100	100	100	100
468	60.2	61.0	30.3	64.0	73.9	53.2
589	4.2	6.6	1.1	7.1	8.3	4.3
605	9.5	12.6	1.4	14.0	13.0	13.0
613	7.5	9.2	0.5	8.4	9.9	5.3

* Given with the reservation that lines widely spaced in energy cannot be accurately compared.

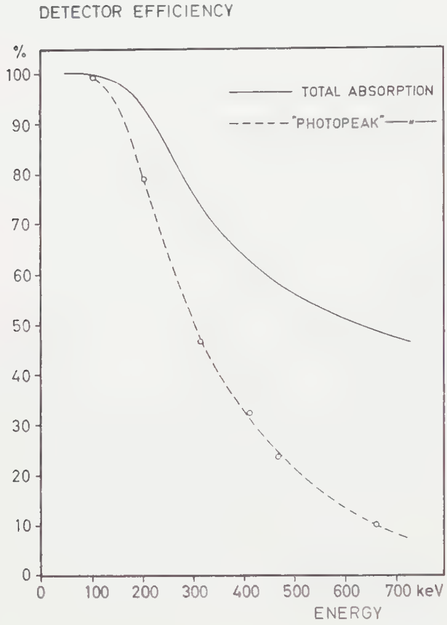

Fig. 11.

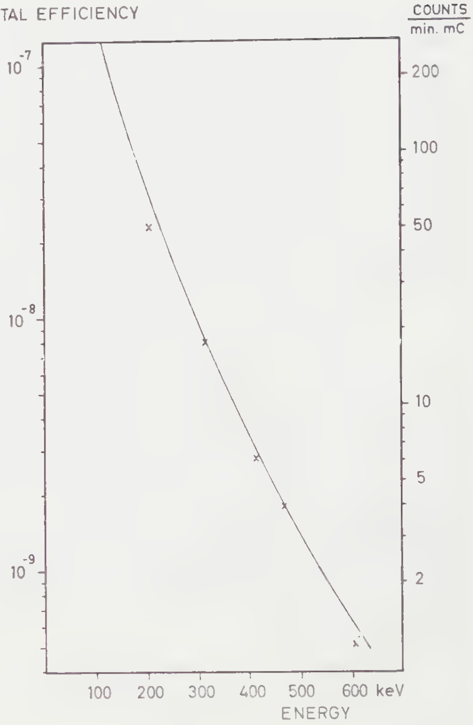

Fig. 12.

Fig. 11. Efficiency curves for the detector, a 1″·1″ NaI(Tl) cylindrical scintillator. The upper curve is taken from ref. [42]. The lower, dashed line is the photopeak efficiency.

Fig. 12. The total spectrometer efficiency. The solid line is obtained as the product of the curves in Figs. 10 and 11, and the effective solid angle. The points represent experimentally obtained counting rates divided by the effective source strength. Self-absorption in the source is neglected, and 0.1 mm source width is assumed. For convenience the efficiency is expressed in two denominations.

denominator is the total number of quanta of a specific energy, emitted by the 0.1 mm wide source. It is easily seen that the total efficiency so defined can also be obtained as the product of Γ, the reflection coefficient (Fig. 10), the detector efficiency (dashed line in Fig. 11), the solid angle and the collimator transmission.

5.1. *Solid angle*

The smallness of the solid angle subtended by the curved crystal from the source is the main cause of the low efficiency of curved crystal spectrometers. As usual, it is the price paid for high resolution. The solid angle in this instrument is equal to

$$6.0 \cdot 10^{-6} \text{ steradians.}$$

The solid angle is not strictly independent of energy, as the source must be moved in order to fulfill the focussing conditions for lower energies. The change is, however, less than 1 % for energies above 40 keV.

5.2. *Collimator transmission*

The geometrical transmission of the collimator is easily calculated and found to be 60 %. From the fact that the transmission curve, Fig. 6, has an extended flat top, we conclude that the actual transmission is the same as the geometrical.

An additional reduction in luminosity is caused by the fact that, unfortunately, only 93 % of the beam hits the NaI crystal because of geometrical conditions.

5.3. *Experimental determination of the total efficiency*

By taking the product of the curved crystal and detector efficiencies and the above mentioned geometrical factors, we obtain the total efficiency of the spectrometer, graphically represented as a function of energy, the solid line in Fig. 12. It is, however, possible to make an independent estimate of the total efficiency from knowledge of the source activity and the peak counting rates obtained experimentally. The activity can be calculated from the amount of source material, the thermal neutron cross section, the thermal neutron flux and irradiation time in the reactor. Furthermore, information about the abundance of the emitted gamma rays is required. This can be found in ref. [45] with sufficient accuracy for two of the isotopes used in this work, Ir^{192} and Au^{198}.

The peak counting rates obtained for the main lines from these isotopes were corrected for source absorption and for the fact that the maximal channel width did not quite encompass the whole of the photopeaks at the higher energies.

From the above considerations the five experimental points in Fig. 12 have been established. The agreement with the calculated efficiency is surprisingly good, and gives strong support to the validity of the efficiency estimates. It should be noted that source absorption has been neglected, and that detector improvements will increase the efficiency at higher energies.

As a summary of the above discussions on relative intensities and efficiencies one might be justified in stating that the high neutron fluxes which will soon be available,[1] will provide the high specific actitivites required for precision measurements of energies of weak lines, and for relative intensity measurements with an accuracy of a few per cent, at least for the strong lines.

ACKNOWLEDGEMENTS

The author wishes to thank Professor Kai Siegbahn for his support and kind interest. It is also a pleasure to express my gratitude to Professor J. W. M. Du Mond, California Institute of Technology for generously giving his expert advice. I am indebted to Dr Carl Nordling for many suggestions, and to members of the nuclear spectroscopy group at this institute, notably Fil. lic. Gunnar Bäckström, for encouraging discussions. The helpfulness of Ing. T. Petersén at the R1 reactor of AB Atomenergi, Stockholm, is gratefully acknowledged.

Institute of Physics, University of Uppsala, Sweden.

---

[1] The Swedish R2 reactor being built in Studsvik, south of Stockholm, is scheduled to operate in 1961 with a thermal neutron flux of 10^{14} neutrons/sec., cm^2, which is 30 times the flux in the R1 reactor which has been available for the present experiments.

REFERENCES

1. Chupp, E. L., private communication.
2. Manning, G., and Du Mond, J. W. M., private communication.
3. Knowles, J. W., Can. J. Phys. *37*, 203 (1959); Knowles, J. W., Chalk River Report GPI-42 (1957) unpublished.
4. Knowles, J. W., Manning, G., Bartholemew, G. A., and Campion, P. J., Phys. Rev. *114*, 1065 (1959).
5. DuMond, J. W. M., Second Annual Report, AEC contract No. AT (04-3)-63 (1956), unpublished.
6. Du Mond, J. W. M., Ann. Rev. Nucl. Sci. *8*, 163 (1958).
7. Du Mond, J. W. M., Proc. Rehovoth Conf. Nucl. Structure 509 (1958).
8. Chupp, E. L., Clark, A. F., Du Mond, J. W. M., Gordon, F. J., and Mark, H., Phys. Rev. *107*, 745 (1957); Chupp, E. L., Du Mond, J. W. M., Gordon, F. J., Jopson, R. C., and Mark, H., Phys. Rev. *112*, 518 and 1183 (1958).
9. Beckman, O., Nucl. Instr. *3*, 27 (1958).
10. Du Mond, J. W. M., Rev. Sci. Instr. *18*, 626 (1947); Du Mond, J. W. M., Ergeb. exakt. Naturw. XXVIII, 232 (1955); Du Mond, J. W. M., Beta- and Gamma-ray Spectroscopy, p. 100, editor K. Siegbahn, North-Holland Publ. Co., Amsterdam (1955).
11. Ryde, N., and Andersson, B., Proc. Phys. Soc. *68B*, 1117 (1955).
12. Lukirskii, P. I., and Sumbaev, O. I., Izv. Akad. Nauk. SSSR Ser. Fiz. *20*, 903 (1956); Sumbaev, O. I., Soviet Physics JETP *5*, 170 (1957).
13. Rose, D., Ostrander, H., and Hamermesh, B., Rev. Sci. Instr. *28*, 233 (1957).
14. Beckman, O., Bergvall, P., and Axelsson, B., Arkiv f. Fysik *14*, 419 (1958).
15. Schult, O., Doctoral thesis, Techn. Hochs. München (1959) unpublished.
16. Barton, G. W., Robinson, H. P., and Perlman, I., Phys. Rev. *81*, 208 (1951).
17. Day, P. P., Phys. Rev. *97*, 689 (1955) and *102*, 1572 (1956).
18. Beckman, O., Axelsson, B., and Bergvall, P., Arkiv f. Fysik *15*, 567 (1959).
19. Sumbaev, O. I., Pribory i Tekh. Éksper. *3*, 27 (1958).
20. Muller, D. E., Hoyt, H. C., Klein, D. J., and Du Mond, J. W. M., Phys. Rev. *88*, 775 (1952).
21. Bergvall, P., Arkiv f. Fysik *16*, 57 (1959).
22. Bergvall, P., and Hagström, S., Arkiv f. Fysik *17*, 61 (1960).
23. Bergvall, P., Hörnfeldt, O., and Nordling, C., Arkiv f. Fysik *17*, 113 (1960).
24. Ingelstam, E., Nova Acta Reg. Soc. Sci. Upsal. Ser. IV, vol. 10, No. 5 (1936).
25. Watson, B. B., West, W. J., Lind, D. A., and Du Mond, J. W. M., Phys. Rev. *75*, 505 (1949).
26. Sandström, A. E., Encyclopedia of Physics, vol. XXX, 78, editor S. Flügge, Springer Verlag, Berlin (1957).
27. Siegbahn, K., and Edvarson, K., Nucl. Phys. *1*, 137 (1956).
28. de Vries, C., Doctoral thesis, Amsterdam (1960).
29. Sokolowski, E., Arkiv f. Fysik *15*, 1 (1959).
30. Andersson, B., Proc. Phys. Soc. *69A*, 415 (1956).
31. Johns, M. W., and Nablo, S. V., Phys. Rev. *96*, 1599 (1954).
32. Baggerly, L. L., Marmier, P., Boehm, F., and Du Mond, J. W. M., Phys. Rev. *100*, 1364 (1955).
33. Davisson, C. H., Beta- and Gamma-ray Spectroscopy, Appendix I, editor K. Siegbahn, North-Holland Publ. Co., Amsterdam (1955).
34. Lind, D. A., West, W. J., and Du Mond, J. W. M., Phys. Rev. *77*, 475 (1950).
35. Sumbaev, O. I., Soviet Physics JETP *5*, 1042 (1957).
36. Hatch, E. N., Doctoral thesis, Cal. Inst. Tech. (1956) unpublished.
37. Beckman, O., Arkiv f. Fysik *9*, 495 (1955).
38. Jaffe, H., Passel, T. O., Browne, C. I., and Perlman, I., Phys. Rev. *97*, 142 (1955).
39. Cochran, A. J., and Ross, M. A. S., Proc. Phys. Soc. *71*, 1011 (1958).
40. Edwards, F., Doctoral thesis, Cal. Inst. Tech. (1960), unpublished.
41. Åström, B., Wapstra, A. H., Thulin, S., and Bergström, I., Arkiv f. Fysik *7*, 247 (1953).
42. Bell, P. R., Beta- and Gamma-ray Spectroscopy p. 133, editor K. Siegbahn, North-Holland Publ. Co., Amsterdam (1955).
43. Vegors, S. H., Marsden, L. L., and Heath, R. L., Philips Petroleum Co., AEC Report IDO-16370.
44. Heath, R. L., Philips Petroleum Co., AEC Report IDO-16408.

45. STROMINGER, D., HOLLANDER, J. M., and SEABORG, G. T., Table of Isotopes, UCRL-1928 (1958).
46. BÄCKSTRÖM, G., Nucl. Instr. *4*, 5 (1959).
47. COHEN, E. R., and DU MOND, J. W. M., Encyclopedia of Physics vol. XXXV, 1, editor S. FLÜGGE, Springer Verlag, Berlin (1955).
48. BECKMAN, O., and BERGVALL, P., Phys. Rev. *114*, 1280 (1959).
49. GERHOLM, T. R., Beta- and Gamma-ray Spectroscopy, Appendix VIII, editor K. SIEGBAHN, North-Holland Publ. Co., Amsterdam (1955).
50. BASHILOV, ANTON'EVA and DZHELEPOV, Izv. Akad. Nauk. SSSR Ser. Fiz. *16*, 264 (1952). Cf ref. [12].

Tryckt den 15 mars 1960

Uppsala 1960. Almqvist & Wiksells Boktryckeri AB